CO-EVOLUTION OF GALACTIC NUCLEI AND GLOBULAR CLUSTER SYSTEMS

OLEG Y. GNEDIN¹, JEREMIAH P. OSTRIKER^{2,3}, SCOTT TREMAINE⁴

Submitted to ApJ

ABSTRACT

We revisit the hypothesis that dense galactic nuclei are formed from inspiraling globular clusters. Recent advances in understanding of the continuous formation of globular clusters over cosmic time and the concurrent evolution of the galaxy stellar distribution allow us to construct a simple model that matches the observed spatial and mass distributions of clusters in the Galaxy and the giant elliptical galaxy M87. In order to compare with observations, we model the effects of dynamical friction and dynamical evolution, including stellar mass loss, tidal stripping of stars, and tidal disruption of clusters by the growing galactic nucleus. We find that inspiraling globular clusters form a dense central structure, with mass and radius comparable to the typical values in observed nuclear star clusters (NSCs) in late-type and low-mass early-type galaxies. The density contrast associated with the NSC is less pronounced in giant elliptical galaxies. Our results indicate that the NSC mass as a fraction of mass of the galaxy stellar spheroid scales as $M_{NSC}/M_* \approx 0.0025\,M_{*,11}^{-0.5}$. Thus disrupted globular clusters could contribute most of the mass of NSCs in galaxies with stellar mass below $10^{11}\,M_{\odot}$. The inner part of the accumulated cluster may seed the growth of a central black hole via stellar dynamical core collapse, thereby relieving the problem of how to form luminous quasars at high redshift. The seed black hole may reach $\sim 10^5\,M_{\odot}$ within $\lesssim 1\,\mathrm{Gyr}$ of the beginning of globular cluster formation.

Keywords: galaxies: evolution — galaxies: formation — galaxies: nuclei — galaxies: star clusters — globular clusters: general

1. INTRODUCTION

The centers of most luminous galaxies contain supermassive black holes (BH) and/or nuclear star clusters (NSC). The history of NSC formation and BH growth can involve a variety of different physical processes. Some of the central stars may have formed in situ, while others may have formed elsewhere and been brought to the center. In this paper we explore the simplest version of the latter hypothesis: that due to dynamical friction, globular star clusters have spiraled from larger radii to the inner few parsecs of a galaxy and there deposited a dense and massive concentration of stars. These stars would form a NSC which, via various dynamical processes, may produce the seed of a supermassive black hole. The timescale for cluster infall and NSC growth, set by the processes of dynamical friction and concurrent tidal disruption, is unrelated to the timescale of accretion growth of the black hole. This difference in the timescales may have important implications for the formation of the first supermassive black holes.

We do not presume the *in situ* and *ex situ* scenarios of NSC formation to be mutually exclusive. The presence of a NSC and/or a BH will attract gas to the central region and induce star formation. This seems to be the case in our own galactic center, where the bulk of the stars are billions of years old but the presence of very massive stars indicates recent star formation.

The idea that globular cluster orbits may decay to the galaxy center by dynamical friction is not new (Tremaine et al. 1975). In a series of papers, Capuzzo-Dolcetta (1993),

Capuzzo-Dolcetta & Miocchi (2008), Antonini et al. (2012), and Antonini (2013) have explored cluster inspiral and disruption leading to the formation of a NSC. Major uncertainties in this analysis are whether there is a pre-existing black hole at the galaxy center and what fraction of the incoming cluster mass, if any, is eventually added to the black hole. Assuming a pre-existing black hole of $4 \times 10^6 M_{\odot}$ at the center of a stellar system resembling the Galactic bulge, Antonini et al. (2012) find that the inspiral of globular clusters could build a significant NSC. Although the observed cluster at the Galactic center contains many young stars that must have formed *in situ*, over half of the cluster could be old ($\sim 10\,\mathrm{Gyr}$) stars acquired from disrupted globular clusters.

This conclusion is consistent with the analysis of the kinematics of two dwarf NSCs by Hartmann et al. (2011); they find that cluster merging can explain most of the kinematic and spectroscopic properties of the NSCs, but that comparable *in-situ* star formation is also required. However, the fraction of *in-situ* stars may increase with the brightness of the NSC: absorption-line spectroscopy of dwarf elliptical galaxies in the Virgo cluster by Paudel et al. (2011) indicates that stars in brighter nuclei have younger ages and higher metallicity than could be contributed by old globular clusters. This trend is also supported by the HST surveys of galaxies in the Virgo and Fornax clusters (Turner et al. 2012). In spiral galaxies, nuclei tend to be smaller and younger in latetype galaxies relative to early-type spirals (Rossa et al. 2006). Leigh et al. (2012) have recently revisited the scaling relations of NSCs and argued that the *present-day* distribution of globular clusters is insufficient to build up the observed nuclei by dynamical friction and disruption. However, they leave open the possibility that the globular cluster systems may have contained more massive and more numerous clusters in the past, which could provide the required stellar material. In fact, the deficit in globular cluster numbers in the central part of our Galaxy, and other galaxies, as compared to the stellar distribu-

¹ University of Michigan, Department of Astronomy, Ann Arbor, MI 48109; ognedin@umich.edu

² Princeton University Observatory, Princeton, NJ 08544

³ Columbia University, Department of Astronomy & Astrophysics, New York, NY 10027

⁴ Institute for Advanced Study, Princeton, NJ 08540

2 GNEDIN ET AL.

tion, can be taken as evidence that dynamical processes have depleted the globular cluster system (e.g., Lotz et al. 2001; Capuzzo-Dolcetta & Mastrobuono-Battisti 2009).

A comprehensive theoretical study of NSC formation by inspiraling clusters was done by Agarwal & Milosavljević (2011). They assumed that all stars in a galaxy form instantaneously in star clusters with a power-law mass distribution having a slope $\beta=2$ between M_{\min} and M_{\max} (cf. eq. 2 below). As massive clusters spiral towards the center, they form a NSC. The steep power-law slope of 2 implied that most of the accumulated mass is from the most massive clusters, and therefore the mass in the inner few pc and the prominence of the NSC depend strongly on the adopted (and largely, unconstrained) value of M_{\max} .

Antonini (2013) further extended that model and explored how the expected NSC properties depend on galaxy mass. He found that the formation of NSCs is suppressed in giant galaxies relative to dwarf galaxies. The absolute normalization of the cluster density profile still remained uncertain because of the unknown cluster formation rate and maximum cluster mass.

Since the mass and spatial distribution of globular clusters are well studied in nearby galaxies, they provide additional, and critically important, constraints on $M_{\rm max}$ and thus on the whole scenario of NSC formation from clusters. In this work we set up a similar calculation to Agarwal & Milosavljević (2011) and Antonini (2013) but choose the parameters to match the observed globular cluster profile in two well-studied galaxies: the Milky Way (MW) and the giant elliptical M87. We also make additional improvements: we account for the observed cosmological evolution of the galaxy stellar profile, model the continuous addition of star clusters over time, and include mass loss due to stellar evolution.

We begin by building a simple model for the formation and evolution of globular cluster systems (§2); a central assumption of this model is that the initial spatial distributions of the clusters and field stars are the same. We then apply this model to the Galaxy, where the most detailed observations are available, in §3. We extend the model to the M87 system in §4 and find that, in order to reproduce the observed distribution of globular clusters, we must account for the evolution of the galaxy structure over cosmic time, in a fashion that matches both recent observational data and cosmological simulations. Once the evolved models match the basic current observed properties of the globular cluster system, we investigate the accumulation of stars stripped from the star clusters at the galaxy center. In §5 we apply this model to scaled-down versions of M87 to investigate how the NSC mass depends on the host galaxy mass. Finally, in §6 we discuss whether the accumulated stellar distribution could undergo collisional evolution and core collapse into a massive black hole rapidly enough to alleviate the timescale problem for high-redshift quasars.

2. A SIMPLE MODEL FOR THE FORMATION AND EVOLUTION OF GLOBULAR CLUSTER SYSTEMS

2.1. Formation

In massive early-type galaxies at the present time, the mass of the globular cluster system is roughly proportional to the total stellar mass, $M_{\rm GC} \sim (1-5) \times 10^{-3} M_*$ (e.g., Spitler & Forbes 2009; Georgiev et al. 2010; Harris et al. 2013). Guided by this relation, we adopt the simple ansatz that in a given galaxy the cluster formation rate was a fixed

fraction $f_{GC,i}$ of the overall star formation rate:

$$\frac{dM_{GC}}{dt} = f_{GC,i} \frac{dM_*}{dt}.$$
 (1)

Specifically, we assume that the globular cluster system forms continuously between redshifts $z_i = 6$ and $z_f = 0$, with the initial density distribution of clusters proportional to the density distribution of field stars formed at the same epoch. This is the simplest assumption; in detail, the cluster fraction may scale with the local gas density (e.g., Kruijssen 2012). Our results are insensitive to the particular choice of z_i , but considering redshifts higher than 6 requires severe extrapolation of the currently available observational scaling relations. By "formation" we include both the *in situ* star and cluster formation, and the accretion of stars and clusters formed in satellite galaxies that later merge with the central galaxy.

To account for the dynamical disruption of globular clusters over time, we choose a larger normalization of the cluster formation rate ($f_{GC,i}$) than the present fraction of stellar mass locked in globular clusters, $f_{GC,f} = (1-5) \times 10^{-3}$. We set $f_{GC,i}$ by matching the final number of clusters in our models for the MW and M87 systems to the observed number.

The masses of individual clusters are drawn from the power-law distribution

$$dN/dM \propto M^{-\beta}, \quad M_{\min} < M < M_{\max},$$
 (2)

that is observed for young massive star clusters in nearby galaxies (e.g., Zhang & Fall 1999; Gieles 2009; Larsen 2009; Chandar et al. 2010a,b, 2011). We adopt the average slope $\beta = 2$, and also explore the effect of varying this slope between 1.8 and 2.2, as allowed by observational uncertainties.

The lower limit of the mass spectrum is set to $M_{\rm min} = 10^4 M_{\odot}$. Most of our results are insensitive to this choice, since we expect all $10^4 M_{\odot}$ clusters (and even most $10^5 M_{\odot}$ clusters) to be dynamically disrupted by the present time.

In contrast, the upper limit of the mass spectrum affects both the shape of the cluster mass function at zero redshift and the total amount of cluster debris accumulated at the center. If we let M_{max} increase to infinity, the mass function would be too broad in most galaxies and the central mass concentration would be too large. By matching the observed mass function, we constrain this important upper limit.

We describe below several galaxy models, appropriate for the Galaxy, the giant elliptical galaxy M87, and scaled-down variants of M87. For the Galaxy, the upper limit of the cluster mass spectrum is taken to be $M_{\rm max}=10^7 M_{\odot}$, while for M87 we increase the upper limit to $2\times 10^7 M_{\odot}$, to account for its broader cluster mass function.

2.2. Disruption

As soon as the clusters have formed, they begin to lose mass via stellar winds and the dynamical ejection of stars through two-body relaxation and stripping by the galactic tidal field.

We model the stellar mass loss using the main-sequence lifetimes from Hurley et al. (2000) and the stellar remnant masses from Chernoff & Weinberg (1990). The time-dependent mass loss rate is calculated as in Prieto & Gnedin (2008). Over 10 Gyr, stellar evolution reduces the cluster mass by up to $f_{\rm se} = 40\%$ for a Chabrier (2003) stellar IMF.

We model the dynamical evaporation of stars in the tidal field of the host galaxy, but not tidal shocks (due, for example, to pericenter passages close to the galactic center) because we do not calculate individual cluster orbits. Effectively, we assume a circular trajectory and take the radius r to be the time-averaged radius of a true, likely eccentric, cluster orbit. A recent estimate of the disruption time based on direct N-body simulations is given by Gieles & Baumgardt (2008). We write it as

$$\frac{dM}{dt} = -\frac{M}{\min(t_{\text{tid}}, t_{\text{iso}})},\tag{3}$$

$$t_{\rm tid}(r,M) \approx 10 \,\text{Gyr} \left[\frac{M(t)}{2 \times 10^5 M_{\odot}} \right]^{\alpha} P(r), \tag{4}$$
$$P(r) \equiv 41.4 \left(\frac{r}{\text{kpc}} \right) \left(\frac{V_c(r)}{\text{km s}^{-1}} \right)^{-1}.$$

Here $V_c(r)$ is the circular velocity of the galaxy at a distance r from its center. The factor P(r) is effectively a normalized period of rotation around the galaxy, which reflects the strength of the local tidal field, which in turn controls the rate of evaporation. Models with $\alpha=1$ and P=1 can reproduce the observed cluster mass function in the Galaxy (e.g., Fall & Zhang 2001; Prieto & Gnedin 2008). However, more recent N-body calculations suggest $\alpha\approx 2/3$ (e.g., Baumgardt 2001; Gieles & Baumgardt 2008) because of the lingering of stripped stars near the tidal radius, and we adopt this lower value for our models.

The formula for $t_{\rm tid}(r,M)$ in equation (3) is derived from N-body models in which the tidal field is strong. However, in the limit of a weak tidal field (which occurs, for example, in the outer galaxy) the evaporation is mostly controlled internally and not by the tidal radius. To account for this, we calculate the evaporation time in isolation as a multiple of the half-mass relaxation time, t_{rh} :

$$t_{\rm iso}(M) = \frac{t_{rh}}{2.5 \, \xi_e} \approx 17 \, \text{Gyr} \left[\frac{M(t)}{2 \times 10^5 M_{\odot}} \right],$$
 (5)

where $\xi_e = 0.0074$ is the Ambartsumian (1938) rate for a single stellar mass model, and the factor 2.5 corrects it for multimass models (e.g., Gieles et al. 2011).

We then take the disruption time for a given cluster to be the smaller of $t_{\rm tid}$ and $t_{\rm iso}$. The isolated evaporation is more important for clusters at large radii and helps to reduce the spatial gradient of the cluster mass function. The weak tidal field regime may be especially relevant for giant galaxies, as recent HST observations of Brodie et al. (2011) indicate that many globular clusters in M87 may not be tidally limited.

When a cluster arrives in the immediate vicinity of the galactic center, the tidal forces may be strong enough to immediately tear apart the whole cluster. This happens when the stellar density at a characteristic place in the cluster, such as the core or half-mass radius, falls below the ambient density (e.g., Antonini et al. 2012). Here we adopt the average density at the half-mass radius as such a density: $\rho_h \equiv \frac{1}{2}M/(\frac{4\pi}{3}R_h^3)$. To estimate the ambient density in the inner galaxy, ρ_* , dominated by stars, we note that the adopted field stellar mass, as well as the calculated mass of the NSC, are increasing with radius roughly as $M_*(r) \propto r^2$, which gives the average density $\rho_*(r) \approx M_*(r)/(2\pi r^3)$. Rewriting this in terms of the circular velocity, we obtain a criterion for direct cluster disruption if

$$\rho_h < \frac{V_c(r)^2}{2\pi G r^2}.$$
(6)

The observed half-mass density of Galactic globular clusters has a wide dispersion, with the median value $\rho_h \sim$

 $10^3 \, M_\odot \, \mathrm{pc}^{-3}$. The density of an individual cluster may depend on its evolutionary stage and location in the galaxy. According to Gieles et al. (2011), star clusters form with a very compact size and then expand until they reach their tidal radius. The expansion phase lasts longer for the more massive clusters than for the less massive ones. During this phase, cluster density scales as $\rho_h \propto M^2$. In later stages of cluster evolution the median density changes slowly and the core of a massive cluster can remain very dense, even when the cluster has expanded to the tidal radius and its outer stars are stripped. Thus it is the median cluster density that determines how long massive clusters could withstand extremely strong tidal forces near the center.

As the NSC begins to build up, its stellar density will exceed even the high density of infalling globular clusters and these clusters will be directly disrupted before reaching the galaxy center. We continuously update the values of $V_c(r)$ to include the accumulated stellar and gaseous debris from the disrupted clusters. We deposit the whole remaining cluster mass at the radius where Equation (6) is first satisfied. To check for this condition, we set a fixed value of $\rho_h = 10^3 \, M_\odot \, \mathrm{pc}^{-3}$ for low-mass clusters ($M < 10^5 \, M_\odot$). For more massive clusters, the density is assumed to vary with mass as $\rho_h = 10^3 \, (M/10^5 \, M_\odot)^2 \, M_\odot \, \mathrm{pc}^{-3}$. In the most massive clusters, we limit ρ_h to a maximum of $10^5 \, M_\odot \, \mathrm{pc}^{-3}$, as it is about the highest observed half-mass density of a stellar cluster. The cluster mass M here is the current value of the mass before disruption, not the initial mass.

2.3. Dynamical Friction

We include the effect of dynamical friction on cluster orbits by gradually reducing the radius r as suggested by Binney & Tremaine (2008), equation (8.24):

$$\frac{dr^2}{dt} = -\frac{r^2}{t_{\rm eff}(r,M)},\tag{7}$$

$$t_{\rm df} = 0.45 \,\rm Gyr \left(\frac{r}{\rm kpc}\right)^2 \left(\frac{V_c(r)}{\rm km \, s^{-1}}\right) \left(\frac{M(t)}{10^5 \, M_\odot}\right)^{-1} f_\epsilon, \quad (8)$$

where we assume a Coulomb logarithm $\ln \Lambda = 5.8$ and take $V_c = \sqrt{2} \sigma$. This expression ignores many uncertain factors, such as the details of stellar velocity distribution and possible variation of the Coulomb logarithm with cluster mass. Our simplified expression suffices for the present calculation, where we also approximate the galaxy stellar mass profile by a single Sérsic model.

We include one important correction for eccentricity of cluster orbits, f_{ϵ} . It is usually parameterized as a function of the ratio of the orbital angular momentum to its maximum value for a given energy, $J/J_c(E)$. Results quoted in the literature range from $f_{\epsilon} \approx (J/J_c)^{0.78}$ (Lacey & Cole 1993) to $f_{\epsilon} \approx (J/J_c)^{0.53}$ (van den Bosch et al. 1999) to $f_{\epsilon} \approx (J/J_c)^{0.4}$ (Colpi et al. 1999). More recent analysis of N-body simulations of the inspiral of a satellite galaxy within its host galaxy by Boylan-Kolchin et al. (2008) found instead $f_{\epsilon} \approx \exp[1.9(J/J_c-1)]$. The differences of the fitting expressions are due to the increasing complexity of the simulations and inclusion of the effects of tidal mass loss of the satellite along its trajectory.

Since we do not know the initial distribution of globular cluster eccentricities, we take as an estimate the distribution of orbit circularity of satellite halos in cosmological simulations

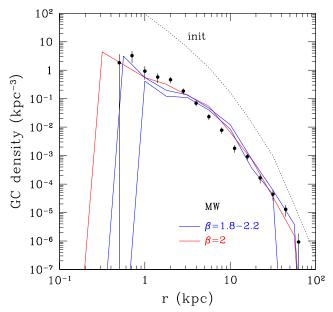


Figure 1. Number density of Galactic globular clusters surviving to the present time, in the fiducial model (red solid line) and its variants with a different slope β (eq. 2) of the initial cluster mass function (blue lines). The dotted line shows the initial distribution of all model clusters at redshift $z_i = 3$; most of these are low-mass clusters that evaporate completely. Symbols with error bars show the observed number density of Galactic globular clusters (from Harris 1996).

of galaxy cluster formation by Jiang et al. (2008). That distribution peaks around $J/J_c(E) \approx 0.5$. Substituting this peak value into the various expressions above, we obtain a range of possible values of the correction factor $f_\epsilon \approx 0.39-0.76$. In order to keep our model simple, we adopt a single value in the middle of this range, $f_\epsilon = 0.5$, for all our calculations. However, it is important to keep in mind the additional uncertainty associated with this factor.

The differential equations for tidal mass loss, stellar mass loss, and dynamical friction are integrated simultaneously. The time step is limited to be 0.02 times the smaller of the current disruption time or current dynamical friction time (we checked that taking a smaller tolerance of 0.01 produces indistinguishable results). We trace the gradual deposition of mass by stripped stars and stellar winds along the cluster path towards the center, and apply dynamical friction only to the remaining bound part of the cluster. Most of the mass loss due to stellar winds happens early in the cluster evolution and that mass is deposited close to the initial location of the cluster. Most of the mass deposited near the galactic center is in the form of stars.

To convert redshift into cosmic time we use the WMAP7 cosmological model, with $\Omega_m = 0.272$, $\Omega_{\Lambda} = 0.728$, h = 0.704. This relation is essentially unchanged with the latest Planck satellite measurements.

3. EVOLUTION OF THE GLOBULAR CLUSTER SYSTEM IN THE GALAXY

We approximate the density distribution of stars in the Galaxy as a spherical Sérsic profile with total mass $M_* = 5 \times 10^{10} M_{\odot}$, effective radius $R_e = 4$ kpc, and concentration index $n_s = 2.2$. We also include a dark-matter halo with an NFW profile having mass $M_h = 10^{12} M_{\odot}$ and scale radius $r_s = 20$ kpc. Our simple mass model satisfies basic observational constraints from Launhardt et al. (2002) within 230 pc, from

McMillan & Binney (2010) at 8 kpc, and from Gnedin et al. (2010) out to 80 kpc from the Galactic center. While we ignore the distinction between the bulge and the disk, the single stellar mass profile should suffice for our calculation of cluster inspiral and disruption because most clusters deposited near the center formed in the inner 1 kpc, where the bulge dominates. We initialize the clusters in a spherical distribution, proportional to that of the field stars, and treat the position r as the time-averaged radius of an assumed orbit, as discussed in §2.3. As a starting point, we take this mass model to be fixed in time from the moment the globular clusters form.

Unlike the elliptical galaxy models described below, for the MW model we choose a single formation epoch for all clusters. We assume that clusters formed at $z_i = 3$ and calculate their evolution for 11.5 Gyr until the present. This assumption is partly justified because most of the observed Galactic clusters are old and metal-poor. The adopted value of z_i should therefore be interpreted as the epoch of the peak of globular cluster formation rate.

Based on the adopted stellar profile, we generate the initial positions of about 8000 model clusters (the exact number depends on the slope β), corresponding to the initial cluster fraction $f_{\text{GC},i} = 0.012$. We construct a fiducial model with $\beta = 2$ and $M_{\text{max}} = 10^7 M_{\odot}$, and variants with $\beta = 1.8$ and 2.2 for the same M_{max} , and with $M_{\text{max}} = 5 \times 10^6 M_{\odot}$ and $2 \times 10^7 M_{\odot}$ for the same $\beta = 2$.

Figure 1 shows the initial and final $(z_f=0)$ radial distributions of the model clusters. Over 97% of the initial clusters are disrupted, but this wholesale destruction is primarily the effect of including low-mass clusters in the initial distribution: all clusters with $M \lesssim 10^5 M_{\odot}$ are disrupted, and therefore the reduction in numbers is dominated by clusters in the range 10^4 – $10^5 M_{\odot}$. More relevant is the consistency of the predicted final distribution with the observed one (from Harris 1996, the updated 2010 edition is at http://physwww.mcmaster.ca/~harris/mwgc.dat). The excellent agreement seen in Figure 1 persists for all considered values of $\beta=1.8$ –2.2 and $M_{\rm max}=5\times10^6$ – $2\times10^7 M_{\odot}$. It is also important to note that the flattening of the observed density profile near the center may be partially due to the distance measurement errors and dust obscuration.

We chose the initial cluster mass fraction to match the normalization of the cluster profile at large radii. Alternatively, Bonatto & Bica (2012) considered several scenarios for the evolution of the cluster mass function and found the best fit for the initial mass of all globular clusters after the gas removal phase ($10^7 \, \text{yr}$) of $M_{GC,i} \sim 3 \times 10^8 \, M_{\odot}$. Our initial cluster mass is a factor of two higher, but that includes also the mass that will be lost by stellar evolution in the first $10^7 \, \text{yr}$. The rest of the difference could be attributed to Bonatto & Bica's choice of lower stellar mass-to-light ratio.

In Figure 2 we show the transformation of the cluster mass function from the initial power law to a roughly lognormal distribution at $z_f = 0$, in satisfactory agreement with the observations. Most of the low-mass clusters have evaporated, and some of the high-mass clusters have spiraled into the center. In order to convert the observed luminosity of Galactic globular clusters into mass, we use two choices for the mass-to-light ratio. In the first, we take a constant $M/L_V = 3\,M_\odot/L_\odot$, as frequently used in the literature for an old metal-poor stellar population. In the second, we take a variable M/L_V , motivated by available dynamical measurements that show M/L_V increasing systematically with

Table 1

System	$M_*(M_{\odot})$	$f_{\mathrm{GC},i}$	$f_{\mathrm{GC},f}$	$M_{10}(M_{\odot})$	$t_{1/2}$ (Gyr)	$R_{\rm h}({\rm pc})$	$R_{\rm h,proj}({ m pc})$	$r_{\rm cc}$ (pc)	$M_{ m BH,exp}(M_{\odot})$	$M_{ m BH,obs}(M_{\odot})$
MW EG2 EG1 M87	5×10^{10} 5×10^{10} 2×10^{11} 8×10^{11}	0.012 0.04 0.04 0.04	0.0012 0.0014 0.0034 0.0054	4.7×10^{7} 1.6×10^{8} 5.0×10^{8} 5.8×10^{8}	0.68 0.20 1.11 1.38	2.8 5.5 7.1 7.4	2.1 5.1 5.3 5.7	9.5 7.0 5.5 5.3	$(2-5) \times 10^4$ $(0.3-2) \times 10^5$ $(1-6) \times 10^5$ $(1-7) \times 10^5$	4×10^{6} $(2 \times 10^{8})^{a}$ $(9 \times 10^{8})^{a}$ $(3.5 - 6) \times 10^{9}$

Columns: M_* – galaxy stellar mass; $f_{\text{GC},i}$, $f_{\text{GC},f}$ – initial and final cluster mass fractions; M_{10} – stellar mass accumulated within inner 10 pc; $t_{1/2}$ – time to reach half of the final mass within 10 pc; R_{h} – half-mass radius of NSC; $R_{\text{h,proj}}$ – projected half-mass radius of NSC; r_{cc} – radius of core-collapsed region at z=0; $M_{\text{BH,exp}}$ – expected black hole mass after core collapse, equation (12); M_{BH} – observed (or inferred) central black hole mass. a The inferred black hole mass is from the scaling relation of Gültekin et al. (2009).

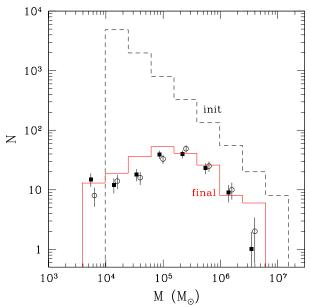


Figure 2. Initial (dashed histogram) and evolved (solid red histogram) cluster mass function in the fiducial Milky Way model. Symbols show the observed mass function of Galactic globular clusters, for two choices of the mass-to-light ratio: constant $M/L_V = 3\,M_\odot/L_\odot$ (open circles), and M/L_V increasing gradually with cluster luminosity (filled squares) as derived using multi-mass King models by Mandushev et al. (1991). Error-bars are from Poisson counting statistics.

cluster luminosity, albeit with large scatter. Most measurements and models (e.g., McLaughlin & van der Marel 2005; Kruijssen & Portegies Zwart 2009) are based on single-mass King (or similar) profiles, which may underestimate the mass-to-light ratio by up to a factor of two, compared to more realistic multi-mass King models, as shown by Mandushev et al. (1991). We adopt the average results of the multi-mass modeling of Mandushev et al. (1991), which can be written as $M/L_V \approx 0.85 \, (L_V/L_\odot)^{0.08}$ in solar units. Kruijssen & Mieske (2009) showed that part of the luminosity dependence arises from preferential escape of low mass stars over the course of dynamical evolution, which is faster in low-mass clusters.

Figure 2 also shows that taking $M_{\rm max} > 10^7 M_{\odot}$ would significantly overproduce the number of high-mass clusters. On the other hand, the case of $M_{\rm max} = 5 \times 10^6 M_{\odot}$ has no clusters with current mass above $2 \times 10^6 M_{\odot}$. Any lower $M_{\rm max}$ would result in a disagreement with observations. Thus our choice of $M_{\rm max} = 10^7 M_{\odot}$ appears to be appropriate for the Galaxy model.

Different slopes of the initial cluster mass function also pro-

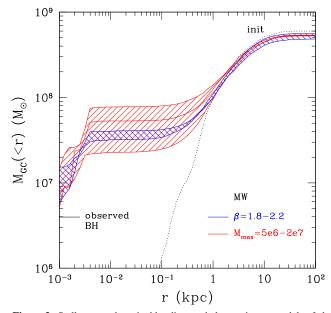


Figure 3. Stellar mass deposited by disrupted clusters in our models of cluster evolution in the Galaxy. The dotted line shows the cumulative mass distribution with radius of the initial cluster population. The blue shaded region shows the cumulative mass of stars from disrupted clusters for models in which the slope of the initial cluster mass function varies in the range $\beta = 1.8 - 2.2$. The red shaded region shows the same quantity when the maximum cluster mass varies in the range $M_{\text{max}} = 5 \times 10^6 - 2 \times 10^7 \, M_{\odot}$. Larger M_{max} results in larger accumulated mass. The observed central black-hole mass is marked at the bottom left part of the plot.

duce noticeable changes in the final distribution. The shallow slope $\beta=1.8$ skews the mass function towards high masses, resulting in 8 clusters with $M>3\times 10^6 M_{\odot}$. The steep slope $\beta=2.2$ pushes in the other direction, lowering the mean cluster mass below $10^5 M_{\odot}$. The fiducial choice $\beta=2$ again matches the data best.

Despite the radial dependence of the evaporation time (equation 4), the peak of the mass function does not show systematic variation with galactocentric radius. The gradient may be difficult to detect because of the low number of surviving clusters in the MW model. The peak mass remains in the range $(1-2) \times 10^5 M_{\odot}$ out to 50 kpc from the center.

Having found a simple model that is consistent with the observed radial distribution and mass function of the Galactic globular clusters, we now calculate the mass of stars deposited by the disrupted clusters (Figure 3). We discount the mass lost via stellar winds, assuming that this is incorporated in the interstellar medium of the Galaxy. Most of the mass loss from

winds takes place when the clusters are young and far from the Galactic center. We also passively evolve the deposited stars to the present, so that the plotted stellar mass is as it would be observed.

Dynamical friction causes massive clusters in the central kpc or so to spiral towards the center. For example, Figure 3 demonstrates that clusters with a combined mass of $4\times 10^7\,M_\odot$ sink to within a few pc of the center. Very close to the center, typically within 10 pc, the clusters completely disrupt so formally the mass does not reach radius r=0. Instead, the stripped stars form a dense stellar core (which we show in Figure 9) whose tidal field in turn disrupts new infalling clusters.

Figure 3 shows that the mass accumulated within a few pc of the Galactic center exceeds the observed mass of the central black hole by a factor of 2–20, depending on the slope β and especially on the maximum cluster mass, M_{max} . More massive clusters spiral in more efficiently, and thus dominate the mass of the stellar nucleus.

Our conclusion that a significant stellar mass can accumulate within the inner few parsecs is similar to that of Antonini et al. (2012), who found that a stream of disrupted massive globular clusters would form a dense core of 1–2 pc in size. They show that such a nuclear cluster would subsequently shrink in size due to gravitational interactions between the stars ("collisional evolution"), to a core radius of about 0.5 pc.

Thus we can draw a robust conclusion that the stellar mass accumulated at the Galactic center is several times larger than the observed black-hole mass. We will investigate the likely state of this stellar nucleus later in §6.

4. EVOLUTION OF THE GLOBULAR CLUSTER SYSTEM IN M87

We assume that the distribution of stars in M87 follows a Sérsic profile with mass $M_* = 8 \times 10^{11} M_{\odot}$, effective radius $R_e = 30 \,\mathrm{kpc}$, and concentration index $n_s \simeq 8$; this fit to the density profile holds over the range $0.7-35 \,\mathrm{kpc}$ (Kormendy et al. 2009). In the innermost kpc the profile flattens to $n_s \approx 3$. However, to obtain an upper limit on the disrupted cluster mass, we adopt a single profile with $n_s = 8$ at all radii. This increases the inner stellar mass by a factor of two within 1 kpc, but only by 8% within 10 kpc. We compare the observed profile with our model at the end of Section 4.6.

We also include a dark-matter halo with an NFW profile having mass $M_h = 2.7 \times 10^{13} M_{\odot}$ and scale radius $r_s = 50 \,\mathrm{kpc}$. This simple two-component model provides an accurate fit to the overall mass distribution obtained by Gebhardt & Thomas (2009) up to 100 kpc.

Based on the adopted stellar profile, we generate the initial positions of $\sim 400,000$ model clusters, corresponding to an initial cluster fraction $f_{GC,i}=0.04$. This is 3–4 times higher than the assumed fraction in the Galaxy, because M87 (like other brightest cluster galaxies) is known to contain proportionately more globular clusters (Harris 2001). In order to match its broader cluster mass function (e.g., Kundu et al. 1999; Waters et al. 2006), we increase the maximum allowed cluster mass to $M_{max}=2\times 10^7 M_{\odot}$.

cluster mass to $M_{\rm max} = 2 \times 10^7 M_{\odot}$. Figure 4 shows the initial $(z_i = 3)$ and final $(z_f = 0)$ density profiles of the model clusters (dashed line), as well as the observed density profile. The latter was deconvolved from the surface number density by McLaughlin (1999) and Tamura et al. (2006). The zero-redshift model is consistent with the observed profile at large radii but underestimates it in the inner several kpc.

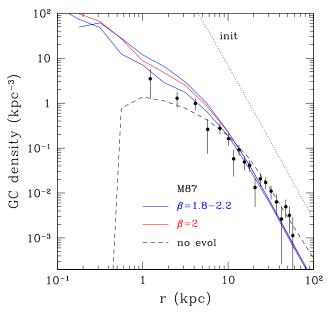


Figure 4. Number density versus radius for the M87 clusters in the fiducial model without evolution (dashed line) and with evolution (solid red line), along with its variants with different slope β (solid blue lines). Symbols with error bars show the observed number density of clusters in M87.

A likely explanation for this discrepancy comes from the observation that elliptical galaxies evolve with redshift, in stellar mass, size, and surface-brightness profile. To take this effect into account, we incorporate the evolution of the galaxy stellar profile and the extended formation of star clusters over the whole cosmic history of the galaxy. In addition, we model the accretion of satellite galaxies as well as their associated black holes and globular cluster systems, as we describe below

4.1. Evolution of the host galaxy

We model the evolution of the stellar distribution of elliptical galaxies like M87 using the parametrization of van Dokkum et al. (2010), which is based on a stacked sample of giant elliptical galaxies in the redshift range 0.2 < z < 2.2. The sample is chosen such that the number density of galaxies $(2 \times 10^{-4} \, \mathrm{Mpc^{-3}})$ is the same at all considered redshifts, and therefore the evolution of mass should reflect the actual growth of the same galaxies, not the changing sample. This method ignores the changes in galaxy numbers due to merging, which are expected to be less significant for these massive galaxies at $z \lesssim 2$, when most of the mass accretion is via minor mergers (e.g., Hopkins et al. 2010; Oser et al. 2012; Leja et al. 2013; Behroozi et al. 2013a). Note that we did not include such evolution in our model of the Milky Way clusters because the relevant data are lacking.

Fitting the photometry of these galaxies to Sérsic profiles, van Dokkum et al. find that the evolution of the total stellar mass, effective radius, and Sérsic index are:

$$M_*(z) = M_*(0) (1+z)^{-0.67},$$

$$R_e(z) = R_e(0) (1+z)^{-1.27},$$

$$n_s(z) = n_s(0) (1+z)^{-0.95}.$$
(9)

The observations constrain these relations only for z < 2.2, but by necessity we extrapolate these relations to higher redshift, which adds uncertainty to our results. Recently, Nipoti et al.

(2012) have derived the evolution of structural parameters of a larger sample of elliptical galaxies in the redshift range z=1.3-2.3, using three different models for the halo mass-stellar mass relation. Our adopted power-law slope for the redshift evolution of stellar mass falls within the range of the slopes (-0.6 to -1.5) derived by Nipoti et al. At low redshift, the increase of the effective radius is consistent with an independent measurement for brightest cluster galaxies, by a factor 1.70 ± 0.15 from $z\approx0.5$ to $z\approx0$ (Ascaso et al. 2011). The adopted evolution is also similar to the build-up of stellar mass in the recent numerical simulations of elliptical galaxy formation by Naab et al. (2009) and Oser et al. (2012).

Although we allow the stellar mass profile to evolve with redshift, we keep the halo mass profile fixed, for several reasons: (i) the inner region of the dark-matter halo has probably stabilized by $z \approx 3$; (ii) the stellar mass dominates over the dark matter mass in the inner 6 kpc, so the exact profile of the inner halo is unimportant; (iii) the region where globular clusters experience significant dynamical friction is even smaller, $\lesssim 1$ kpc (see Figure 7), and hence even more strongly dominated by the stellar mass.

We use the evolving stellar profile to calculate the circular velocity $V_c(r,t)$ that enters the disruption time and dynamical friction calculation (equations 3 and 7).

4.2. Accretion of satellite galaxies

The growth in stellar mass over cosmic time described by equation (9) can be crudely divided into two channels: stars that form in the main body of the elliptical galaxy (in situ growth) and stars that are brought in by accreting satellite galaxies ("accretion" growth). The exact breakdown between these two channels is not known. However, van Dokkum et al. (2010) estimate that at $z \gtrsim 1-2$ the central galaxy produces the majority of stars, while at lower redshifts satellite accretion dominates the stellar mass build-up. Similar conclusions were reached by Oser et al. (2010) by analyzing numerical simulations of galaxy formation.

We have approximated the relative contribution from each channel by fitting the observed trends in van Dokkum et al. (2010) to growth rates of the form $dM_*/dt \propto (t/\tau) \ e^{-t/\tau}$, where time t is measured from the Big Bang. We find $\tau \approx 1.1 \, \text{Gyr}$ for *in-situ* growth and $\tau \approx 6 \, \text{Gyr}$ for accretion growth. Figure 5 shows the fractional contribution of each channel to the total stellar mass.

4.3. Continuous formation of clusters

Given the evolution of the overall stellar component, we allow for continuous (rather than instantaneous) formation of star clusters. In order to consider the earliest formation of clusters, we extend the initial epoch to $z_i = 6$. The details and exact timing of globular cluster formation are still poorly understood and it may be desirable to consider even earlier epochs, however further extrapolation of the scaling relations (Equation 9) is extremely uncertain.

We split the cosmic time between z_i and $z_f = 0$ into 20 equal-duration intervals (of 640 Myr) and form a group of clusters in each interval. The total mass of the group formed in each interval is proportional to the increase of stellar mass within that interval: $\Delta M_{GC} = f_{GC,i} \Delta M_*$, with the same factor $f_{GC,i}$ as before. This algorithm produces the same number of clusters as in the instantaneous model, but now their formation is distributed over the Hubble time. In each interval, the new clusters are added according to the spatial profile of the field stars at that epoch.

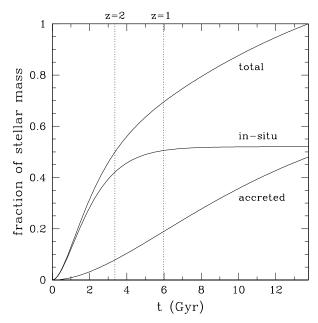


Figure 5. Growth of stellar mass in an average elliptical galaxy, based on the analysis of van Dokkum et al. (2010). The plot shows the fraction of the z=0 mass accumulated at a given cosmic time, measured from the Big Bang. The *in-situ* stars are those formed in the main galactic system, typically within $\sim 10\,\mathrm{kpc}$ from the center. The "accreted" stars are brought in by mergers and disruption of satellite galaxies, typically from larger distances.

Some of the clusters in each group form *in situ* and some come from accreted satellites. Since the accretion events are not actual star formation but the addition of already existing stars, we assign a formation epoch for the accreted clusters that differs from the time of accretion. Specifically, we draw an epoch prior to accretion, from the distribution of the satellite's star formation history, assuming it is the same as for the central galaxy (Figure 5). The dynamical evolution of the satellite clusters prior to accretion is calculated simply using Equation (5), thus ignoring tidal truncation. The initial location of the satellite clusters is also not important, as they are added later to the central galaxy along with the other satellite stars. After accretion the satellite clusters are subject to the same dynamical friction and evolution as the *in-situ* clusters.

We also ignore potential migration of old clusters as the host galaxy's stellar mass grows. If the existing clusters were on circular orbits and conserved their angular momentum, their orbital radius would shrink as the mass interior to the orbit grows. On the other hand, mergers that lead to the increase of the stellar effective radius should excite the orbits of the old clusters to larger radii. It is not clear where the sum of the two effects would point. In view of these uncertainties, we do not adjust the positions of the old clusters as the galaxy grows, and only include the monotonic effect of dynamical friction.

4.4. Evolution of the cluster mass function

Many studies of the dynamical evolution of globular clusters have demonstrated that the cluster mass function develops a characteristic peaked shape as a result of preferential disruption of low-mass clusters (see, e.g., review by Portegies Zwart et al. 2010). Our model similarly transforms the initial power-law mass function into a peaked distribution, well fit by a log-normal function. We have already shown this in the case of the Galaxy (Figure 2). For M87, the peak mass

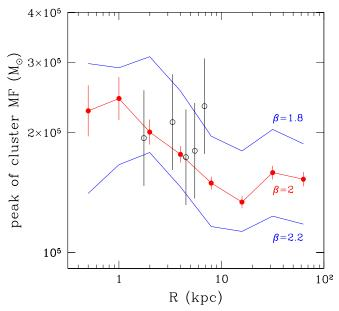


Figure 6. Peak of the projected mass function of clusters in the M87 system (solid red symbols with error bars), as a function of cylindrical distance from the galaxy center. Blue lines show the possible range due to the variation of the slope of the initial cluster mass function β between 1.8 and 2.2. Open black circles with errorbars show the observed peaks from Kundu et al. (1999) and their 1σ errors.

 $\log M_{\rm peak} \approx 5.2$ matches the observations in the inner regions (Waters et al. 2006). However, the model mass function is somewhat broader than the observations, with a log-normal standard deviation $\sigma_M = 0.75$ dex compared to the observed value $\sigma_M = 0.57$ dex for clusters located between 1 and 9 kpc of the galaxy center (Kundu et al. 1999).

We have also checked that the case of $M_{\rm max}=10^7\,M_{\odot}$, as in the Galaxy model, results in no clusters with current mass above $4\times10^6M_{\odot}$, whereas the data require at least a dozen of more massive clusters. This justifies raising the maximum cluster mass in the M87 model to at least $2\times10^7M_{\odot}$.

Faster disruption of low-mass clusters in the inner parts of the galaxy leads to an increase of the average mass of surviving clusters as we approach the center. To compare this prediction for M87 with the HST observations of Kundu et al. (1999), we have randomly projected cluster positions in our model and calculated the peak of the cluster mass function in bins of cylindrical radius *R*. Figure 6 shows the gradient of the peak mass in the model and the absence of such a gradient in the observations, but the observational errors are large enough that the predictions are still statistically consistent with the data.

4.5. Accretion of satellite black holes

Most massive galaxies in the local universe appear to contain a massive black hole at their center. The satellites accreted by our central galaxy are also likely to bring with them their black hole. We add these satellite black holes to the host galaxy at the time of accretion and then follow their inspiral towards the center.

For simplicity, we attribute all the accreted mass in a given 640 Myr interval to a single satellite, which would contribute one black hole. We estimate the mass of the latter using the observed relation between black-hole mass and host galaxy

luminosity at $z \approx 0$ (Gültekin et al. 2009):

$$M_{\rm bh} \approx 9 \times 10^8 M_{\odot} \left(\frac{L_V}{10^{11} L_{\odot}}\right)^{1.1} f_{\rm bh}(z).$$
 (10)

Assuming a stellar mass-to-light ratio $M_*/L_V = 2M_{\odot}/L_{\odot}$, we obtain $M_{\rm bh,sat}/M_{*,\rm sat} \approx 0.004$ in the relevant mass range $(M_* \gtrsim 5 \times 10^{10} M_{\odot})$. This ratio would be correspondingly lower if we had chosen a higher value of M_*/L_V . Current observational constraints from Sani et al. (2011) give the black hole mass fraction between 0.001 and 0.004, although Kormendy & Ho (2013) and Graham & Scott (2013) have recently advocated that this should be revised upward to about 0.005. Our choice of M_*/L_V is therefore consistent with the observed range.

Black holes added at redshift z>0 would have smaller masses because they have had less time to grow. We account for this effect by the factor $0 \le f_{\rm bh}(z) \le 1$, taken to be the fraction of the overall cosmic black hole density attained at the accretion epoch, using Figure 1 from Yu & Tremaine (2002). This fraction is $f_{\rm bh}\approx 0$ at z>6, and it rises monotonically to $f_{\rm bh}=1$ at z=0.

Our algorithm gives the maximum contribution of satellite black holes. If we were to split the accreted mass in several satellites, it would slightly reduce the combined black hole mass at the center of the main galaxy, because dynamical friction is less efficient for smaller black holes.

In order to determine where to place a satellite black hole at the time of accretion, we calculate the radius where the enclosed added stellar mass is 0.004 of the total added stellar mass. This implies that these black holes are deposited along with the innermost satellite stars, which are likely to be gravitationally bound to them. We then follow the orbital evolution of the satellite black holes due to dynamical friction, again including the factor $f_{\epsilon} = 0.5$ describing orbit eccentricity, until they sink to the galactic center.

The details of satellite black hole orbits do not affect the stellar mass accumulated at the center from disrupted globular clusters. We have checked that the accumulated mass is not visibly changed even if we move the black holes to the center as soon as the satellites are accreted onto the host galaxy.

4.6. Results

We now discuss the results from the model for the evolution of M87, its globular clusters, and its satellites described in $\S\S4.1-4.5$. First consider Figure 4, showing the radial distribution of the globular clusters at the present time. The dashed line, from the model with no evolution of the galaxy, underestimates the observed cluster density profile, as we noted just before the start of $\S4.1$. After including evolution, the model now overestimates the density in the inner $\sim 2\,\mathrm{kpc}$. At large radii the model cluster profile now falls systematically below the observed profile but is still consistent with it within the errors. Thus the inclusion and exclusion of the evolution brackets the actual cluster distribution, which suffices for the purpose of our models.

Figure 7 shows the cumulative mass of disrupted clusters in the M87 models that include galaxy evolution. The stellar mass accumulated within 10 pc of the center is a factor of ten below the black-hole mass measurement from stellar dynamics by Gebhardt et al. (2011): $M_{\rm bh,M87} = (6.6 \pm 0.4) \times 10^9 M_{\odot}$. However, the discrepancy is less with the black-hole mass based on gas-dynamical measurements (Walsh et al. 2013): $M_{\rm bh,M87} = (3.5^{+0.9}_{-0.7}) \times 10^9 M_{\odot}$.

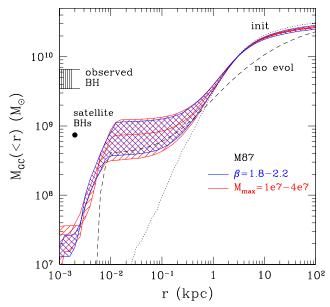


Figure 7. Stellar mass deposited by disrupted globular clusters in our M87 models. The line notation is as in Figure 3. The red shaded region corresponds to the range $M_{\rm max} = 10^7 - 4 \times 10^7 \, M_{\odot}$. The dashed line shows the case without evolution of the galaxy, while the solid lines include evolution. The filled circle shows the sum of the masses of all black holes in satellite galaxies brought in to the center by dynamical friction. The observed black hole mass measurements differ for the stellar-dynamics and gas-dynamic methods and are shown as a shaded range.

In the model without evolution, the accumulated mass is even lower (by 40% in the fiducial model). Within 1 pc, the accumulated mass falls by another order of magnitude in the model with evolution, and essentially vanishes without evolution

The plot also shows the cumulative mass of the satellite BHs that have sunk to the center by dynamical friction. These contribute a mass that is comparable to the mass that accumulates in the center from globular clusters, but still is insufficient to provide the majority of the observed black-hole mass.

The sharp drop of the accumulated mass profile at $r < 10 \,\mathrm{pc}$ is due to the formation of a dense NSC. The tide from the NSC disrupts globular clusters as they approach the center; roughly speaking, as the NSC accumulates mass it grows in radius so that its mean density remains comparable to the mean density of the clusters it destroys. In the inner few parsecs the space density of the NSC reaches $\sim 2 \times 10^5 M_{\odot} \,\mathrm{pc}^{-3}$, while the projected surface density reaches $\sim 5 \times 10^6 M_{\odot} \,\mathrm{pc}^{-2}$.

Figure 8 shows the build-up of the stellar surface density with time. The material lost in stellar winds is deposited early, and close to the initial location of the clusters, but some gas is contained within the NSC by continuous mass loss from the accumulated stars. This gas may contribute to *in situ* star formation that is required to explain the blue colors of some NSCs. The sharp upturn of the stellar density at 10 pc corresponds roughly to the radius of the NSC composed of stars from disrupted clusters. A significant fraction of the NSC is accumulated already by cosmic time t = 2 Gyr ($z \approx 3.3$).

The observed surface brightness of M87 (Kormendy et al. 2009) flattens in the inner 0.7 kpc relative to our adopted single Sérsic profile. Such flattenning is likely to develop because of the scattering of stars away from the center by merging supermassive black holes, even if the initial stellar density was higher. In our models we do not consider the dynamical

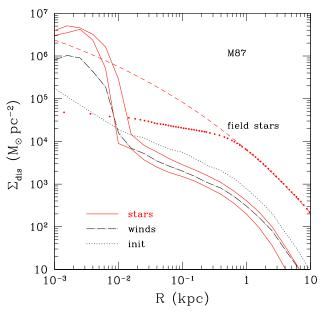


Figure 8. Projected surface density of stars in the M87 model at z = 0. Dashed red line is the adopted field star profile; the observed surface brightness (from Kormendy et al. 2009) flattens in the inner 0.7 kpc and is shown by filled symbols. Dotted black line is the combined initial profile of all model clusters. Solid red lines show the growth of the density of stripped stars: at cosmic time t = 2 Gyr (lower line) and at present (upper line). The dot-dashed black line shows the cumulative density of stellar winds ejected from the clusters by the present time. Some of this gas could be processed into the *in situ* star formation.

effects of supermassive black holes, focusing instead on the early stages when the build-up of NSC could produce a seed for the central black hole. If we used a double Sérsic profile, with a break at 0.7 kpc, the accumulated NSC could be smaller, but it is less clear how the contrast with the field density would change. The use of a single Sérsic profile allows us to include galaxy evolution, described by Equation (9). The data are currently lacking to describe the evolution of a broken profile, and therefore, in this case the formation history of the globular cluster system is unconstrained.

5. LOWER-MASS ELLIPTICAL GALAXIES

The stellar debris accumulated in the central few pc is less massive than the observed black hole in M87, while it is the opposite in the model of the Galaxy. To explore further the dependence of the NSC mass on host galaxy properties, we consider two scaled-down versions of the M87 system. The first (EG1 model) has stellar mass 4 times lower than M87, the other (EG2 model) has stellar mass 16 times lower than M87 and similar to the Milky Way. The other parameters for the two models are set using the observed galactic scaling relations (e.g., Guo et al. 2009): $n_s = 4$, $R_e = 8.6$ kpc, $M_h = 5 \times 10^{12} M_{\odot}$, $r_s = 35$ kpc for EG1, and $n_s = 2$, $R_e = 2.5$ kpc, $M_h = 10^{12} M_{\odot}$, $r_s = 20$ kpc for EG2. These undergo the same evolution with redshift as the M87 model above. We also keep the same initial fraction of globular clusters and slope of the initial mass function that we used for the M87 model, $f_{GC,i} = 0.04$, $\beta = 2$. The maximum cluster mass is $M_{\rm max} = 2 \times 10^7 M_{\odot}$ for EG1, the same as in our M87 model, while for EG2 $M_{\text{max}} = 10^7 M_{\odot}$, the same as in our Galaxy model. Since we do not have observed samples of globular clusters for these new models, our choice of $M_{\rm max}$ is motivated by similarity of the galaxy stellar mass.

GNEDIN ET AL.

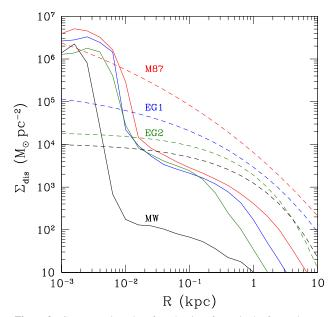


Figure 9. Current projected surface density of stars in the four galaxy models. Solid lines show the stars stripped from disrupted globular clusters, evolved to z = 0; dashed lines show the adopted field stellar profile.

Table 1 shows the surviving cluster fraction and the accumulated stellar mass in these cases. The expected black-hole mass in these two systems is derived from the scaling relation of Gültekin et al. (2009). Viewed together, our four galaxy models exhibit a clear trend: the stellar mass in disrupted globular clusters that can accumulate within a few parsecs of the center is larger than the observed black hole mass in low-luminosity galaxies, and smaller in high-luminosity galaxies, with the crossing point at stellar mass of about $10^{11} M_{\odot}$ in the spheroidal component.

Note that the EG2 model has a significantly more massive nuclear cluster than the Galaxy model, despite the same total stellar mass. Only part of the difference is due to the higher initial fraction of globulars in EG2. If we reduce the initial cluster fraction in the EG2 model to that of the MW model (from 0.04 to 0.012), the accreted mass at 10 pc scales down proportionally by a factor of 3.3. However, this does not work the opposite way. If we increase the initial fraction of the MW clusters to 0.04, the accreted mass at 10 pc increases only by a factor of 1.7. This asymmetry is due to the different structure (larger effective radius R_e) of the late-type MW model compared to the early-type EG2 model.

6. IMPLICATIONS FOR THE FORMATION OF NUCLEAR STAR CLUSTERS AND CENTRAL BLACK HOLES

Rapid accumulation of globular cluster debris at the galaxy center leads to the build-up of a massive and prominent NSC. In this section we discuss how the predicted properties of these NSCs compare with the observations of such clusters in nearby galaxies.

Figure 9 compares the prominence of the NSC for all four of our galaxy models. In all models it rises over the field stars only in the inner 10 pc. However within that region, in all models but M87 it dominates in surface brightness by one or two orders of magnitude. Thus these NSCs could be easily observable given sufficient spatial resolution. One potential caveat is that if mergers of supermassive black holes happen after the NSC formation, the central density may be signifi-

cantly reduced.

In the MW model, the projected density at our innermost radius, 1 pc, is about $10^6 M_{\odot} \,\mathrm{pc}^{-2}$, while the average space density within 1 pc is $2 \times 10^5 M_{\odot} \,\mathrm{pc}^{-3}$. Both values are within a factor of two of the density of the Galactic NSC (Schödel et al. 2007; Oh et al. 2009), which we consider to be excellent agreement given the modeling and observational uncertainties. However, the model predicts a sharper rise of the NSC density than observed. The mass contained within 10pc of the Galactic center is measured to be $\approx 3 \times 10^7 M_{\odot}$ (e.g., Schödel et al. 2007; Merritt 2010), while our model overestimates it by 50% (see Table 1). Our results could be reconciled with observations if this mass was distributed over a few tens of parsecs instead, as would be the case if we overestimated the efficiency of dynamical friction near the Galactic center. It is also possible that our adopted model for the field star distribution near the center underestimates the actual density of stars, which makes the rise of the NSC density in the inner 4 pc more pronounced than observed.

In the M87 and EG1 models, the maximum surface density is $\sim 4 \times 10^6 M_{\odot} \, \mathrm{pc}^{-2}$. At 10 pc, roughly the extent of the NSC, the projected density for all three elliptical models is in the range $\Sigma_{\rm dis}(10\,\mathrm{pc})=10^4-10^5 M_{\odot}\,\mathrm{pc}^{-2}$. These values fall right in the middle of the observed distribution of surface density (measured at the effective radius) of the most massive NSCs ($M_{\rm NSC}=10^7-10^9 M_{\odot}$) in both nearby late-type galaxies (Hartmann et al. 2011) and in early-type galaxies with $M_*<4\times10^{10} M_{\odot}$ in the Virgo and Fornax clusters (Turner et al. 2012), as well as ultracompact dwarf galaxies (Misgeld & Hilker 2011).

Our results also compare favorably with the observed fraction of galaxy stellar mass contained in its NSC. While the compilations of Seth et al. (2008) and Scott & Graham (2013) show a wide variation from galaxy to galaxy, the median value is 2×10^{-3} for early-type spheroidal galaxies, and around 3×10^{-4} for spirals. Turner et al. (2012) find a mean value of $(3.6 \pm 0.3) \times 10^{-3}$ for early-type galaxies in the Virgo and Fornax clusters. Taking the mass enclosed within $10 \text{ pc} \ (M_{10})$ as an estimate of the NSC mass, our models M87, EG1, and EG2 give the expected values, $M_{10}/M_* = (1-3) \times 10^{-3}$. However, there is a trend of the ratio M_{10}/M_* decreasing with galaxy mass, which we discuss in Section 6.3.

Based on these comparisons of the mass and density, we conclude that our models predict the build-up of realistic NSCs from the stars brought in by infalling globular clusters. These old stars may not explain the blue colors of many NSCs which indicate an additional younger population, but they provide sufficient potential well for the interstellar gas to condense and form new stars.

6.1. Mass of the Nuclear Star Cluster

It may be useful to provide a simple estimate of the accumulated stellar mass in our model. As a rough guess, we can assume that all globular clusters with the initial dynamical friction timescale shorter than the Hubble time will spiral into the center. We also note that the initial cluster distribution mirrors the field stellar distribution, and therefore we can integrate the galaxy stellar mass enclosed within a typical radius of inspiral for globular clusters. Since clusters lose mass along the way by tidal disruption and stellar evolution, we need to reduce our estimate by a typical factor of 0.25 that corresponds to this mass loss. The accumulated mass of the

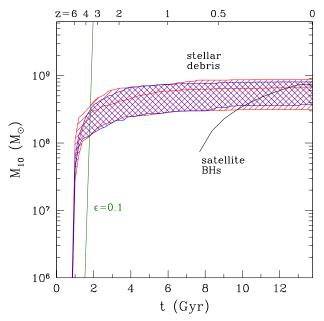


Figure 10. Stellar mass accumulated within 10pc in the M87 system, assuming that the globular clusters begin forming at $z_i = 6$. Line notation as in Figure 7. The solid black line shows the cumulative mass of central black holes from the accreted satellite galaxies. The straight green line indicates the growth of a hypothetical $10\,M_\odot$ stellar black hole by continuous Eddington-limited accretion with the radiative efficiency $\epsilon = 0.1$, starting at $z_i = 6$.

NSC is then

$$M_{NSC} \approx 0.25 \, f_{GC,i} \, M_* (< r_{df}).$$
 (11)

We have found empirically that a radius $r_{\rm df} \approx 1.4 \, \rm kpc$ gives a good estimate for the fiducial models ($\beta = 2$, $M_{\rm max} = (1-2) \times 10^7 \, M_{\odot}$), to within a factor of 2 of the full models. Starting at such a radius in our elliptical galaxy models, a $2 \times 10^6 \, M_{\odot}$ cluster would spiral into the center in a Hubble time.

6.2. Possible Collapse to a Black Hole

Figure 10 shows the growth with cosmic time of the mass of stripped stars accumulated within the inner 10 pc of M87. Most of the mass is assembled by z = 2, and a significant fraction already by $z \sim 4$. This is significantly faster than the growth of the total stellar mass of the galaxy.

Note that we begin the calculation of cluster evolution at $z_i = 6$, and therefore the central mass accumulation begins only from that epoch. We did not model earlier epochs because the extrapolation of the observed galaxy evolution would be extremely uncertain. Nevertheless, it is likely that the mass began accumulating at an even higher redshift. This accumulation would happen on a timescale shorter than that of radiative accretion, and therefore may have important implications for the massive black holes powering the earliest known quasars, as was first suggested by Capuzzo-Dolcetta (1993). For illustration we show the growth of a hypothetical $10M_{\odot}$ stellar black hole by continuous Eddington-limited accretion. We take a typical value of the radiative efficiency for non-rotating black holes, $\epsilon = 0.1$, which gives the exponential growth (Salpeter) time $t_S = 4.5 \times 10^8 \, \epsilon / (1 - \epsilon) \, \text{yr} =$ 5×10^7 yr. Such a black hole would reach the mass of $10^9 M_{\odot}$ in $t_S \ln(10^9/10) \approx 9 \times 10^8$ yr. In case of the maximum radiative efficiency for a rotating black hole, $\epsilon \approx 0.3 - 0.4$ (Thorne 1974; Noble et al. 2009), the timescale is 4–6 times longer. In

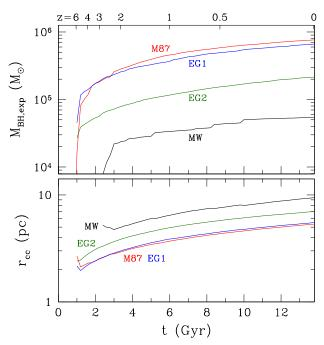


Figure 11. Evolution of the radius of core collapsed region (bottom panel) and the expected mass of a black hole formed within it (top panel), according to the estimate given in §6.2 and Equation (12).

either case the initial mass accumulation by infalling globular clusters is faster. If this process could create massive black holes quickly, it would alleviate the timescale problem posed by the existence of quasars at redshift 7, when the Hubble time is less than 0.8 Gyr.

Once a massive NSC forms, its subsequent evolution can indeed produce a seed black hole at the center. Miller & Davies (2012) argue that a cluster with high enough velocity dispersion $\sigma \gtrsim 40 \, \rm km \, s^{-1}$ will inevitably form a black hole because kinematic heating from binary stars is insufficient to prevent complete core collapse. Collisions between binary and single black holes (products of the evolution of massive stars) will remove them from the cluster core after $10^8 - 10^9$ yr, via either three-body kicks or the asymmetric emission of gravitational radiation. At the end of this phase, only one black hole is expected to remain at the center and grow by tidally disrupting and absorbing other stars in the collapsing core. Even if no black hole remains after the violent kicks, runaway mergers of main-sequence stars will create a single central black hole. Miller & Davies (2012) estimate that the subsequent black hole growth will be fast until the energy of stars within its sphere of influence is sufficient to hold off collapse. The expected black hole mass at the end of the consumption process is given by their Equation (13), re-written here as

$$M_{\rm BH,exp} \sim 700 M_{\odot} \left(\frac{\sigma}{40 \,\rm km \, s^{-1}}\right)^{4/3} \left(\frac{M_{NSC}}{10^6 M_{\odot}}\right)^{2/3}.$$
 (12)

This is a significant boost for growing a supermassive black hole in galactic nuclei, compared to a typical stellar mass.

There are several uncertainties underlying the above argument. The growth of the runaway merger product may be limited by strong stellar winds, removing the bulk of the mass and leaving a black hole of only $\sim 10\,M_{\odot}$ for solar-metallicity stars (Glebbeek et al. 2009). However, the extrapolation of the wind model of main-sequence stars may not apply to the

12 GNEDIN ET AL.

inhomogeneous envelope surrounding merged stellar cores. Also, the effect of the winds is reduced at the low metallicity characteristic of globular cluster stars. In any case, a black hole of some substantial mass is expected to form at the center and to proceed to grow by disrupting and accreting main-sequence stars.

Another uncertainty concerns the initial phase when stellarmass black holes eject each other, until the last one remains to dominate the core. If the energy generated in three-body encounters between binary and single black holes is efficiently transferred to the velocities of main-sequence stars, core collapse could be delayed by several relaxation times, until all black holes are gradually ejected (Breen & Heggie 2013b). At present, the value of the delay time is uncertain, as N-body simulations show that it keeps decreasing, by a factor of several, with increasing range of mass of main-sequence stars included in the simulation (Breen & Heggie 2013a). Low velocity dispersion clusters may indeed retain significant numbers of black holes for several relaxation times (Sippel & Hurley 2013; Morscher et al. 2013), but a fully realistic simulation for a high dispersion cluster ($\sigma > 40 \,\mathrm{km \, s^{-1}}$) is not yet available. However, as long as one black hole dominates cluster core, the potential presence of smaller black holes does not change our argument about runaway growth.

Additional delay of core collapse could be caused by kinematic heating by the rest of the host galaxy. We can estimate this delay by considering the ratio of the nuclear relaxation time to the heating time, using the scaling given by equation (10) of Merritt (2009): $t_{\rm rh}/t_{\rm heat} \sim (M_*/M_{NSC})^{1/2}(R_{NSC}/R_e)^{5/2} \sim 10^{-6}$, with the typical parameters of NSC and host galaxy from Table 1. This ratio is so small that we can ignore the interaction of NSC with its host galaxy.

In the following discussion we assume that the delay is smaller than the collapse time of remaining main-sequence stars within the NSC. The core collapse time depends on cluster concentration and stellar mass spectrum (e.g., Gnedin et al. 1999). Direct N-body simulations of Portegies Zwart & McMillan (2002) and Monte Carlo simulations of Gürkan et al. (2004) show that the most massive component reaches the center within a fraction of the half-mass relaxation time, typically $t_{cc} \sim 0.2 t_{rh}$. We use our predicted NSC profile to calculate the relaxation time as a function of distance from the center, assuming an average stellar mass of $1 M_{\odot}$ and the Coulomb logarithm $\ln \Lambda = 12$. The size of the nuclear region r_{cc} that would collapse on a timescale shorter than the current age, $t_{cc}(r_{cc}) \equiv t$, is shown in the bottom panel of Figure 11.

Within $\lesssim 1$ Gyr after the beginning of globular cluster formation, this region includes a large part of the NSC. The time to accumulate half of the final NSC mass ranges from 0.2 Gyr for the small EG2 galaxy model to 1.4 Gyr for the giant M87 galaxy model. The core collapsed region quickly reaches 2–3 pc in radius in the early-type models, where the half-mass radius of the whole NSC is 5–7 pc (Table 1). It is then possible that these dense systems undergo catastrophic core collapse and produce a seed black hole, as described by Miller & Davies (2012). We estimate the expected black hole mass using Equation (12) with the estimated parameters of NSCs in our models. These masses are plotted in the top panel of Figure 11 and reach $(0.3-1) \times 10^5 M_{\odot}$ by $z \approx 5$.

The collisional evolution appears to be slower in the MW model, but this is an artifact of our starting the calculation at

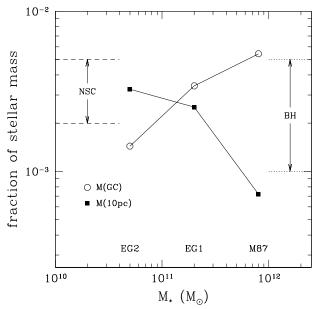


Figure 12. Scaling with galaxy mass of the fractions of surviving globular clusters and nuclear star cluster within 10pc, for the three early-type galaxy models. Horizontal dashed lines on the left show the median range of NSC mass fraction for galaxies in the local neighborhood and the Virgo and Fornax clusters, from Seth et al. (2008); Turner et al. (2012); Leigh et al. (2012); Scott & Graham (2013). Horizontal dotted lines on the right show the range of the central black hole mass fraction, from Sani et al. (2011); Kormendy & Ho (2013); Graham & Scott (2013).

a later epoch of $z_i = 3$. This arbitrary choice was forced by the lack of information on the early evolution of the Galaxy; in reality the build-up of the NSC should begin earlier. The core collapsed region in the MW model includes essentially the whole NSC, because it is smaller than in the elliptical models. The seed black hole mass could reach $(2-5) \times 10^4 M_{\odot}$.

6.3. Scaling with Host Galaxy Mass

Figure 12 shows the scaling of our results with galaxy mass. The fraction of stellar mass contained in the NSC is a decreasing function of M_{\ast} for the three early-type models. It can be approximately described by the following relation

$$M_{NSC}/M_* \approx 0.0025 M_{*,11}^{-0.5},$$
 (13)

where $M_{*,11}$ is the galaxy stellar mass in units of $10^{11} M_{\odot}$, and we take M_{10} to be a proxy for M_{NSC} . Using the fundamental plane scaling of galaxy stellar mass with velocity dispersion, σ_g , this relation translates to $M_{NSC} \propto \sigma_g^{1.5-2}$. It is interesting to note that the MW model also satisfies this relation if by M_* we take only the mass of the bulge, that is, a spheroidal component similar to the early-type models.

Antonini (2013) also considered the scaling of NSC mass with galaxy velocity dispersion and found $M_{NSC} \propto \sigma_g^{3/2}$, in the model without a pre-existing central BH. His relation is consistent with ours and supports the idea that NSC formation is more efficient in lower-mass galaxies. If the central BH already exists at the time when a NSC is built-up, Antonini (2013) finds that the NSC mass would be suppressed even further. This view is supported by observations of Neumayer & Walcher (2012) that a supermassive black hole, when present, may limit the NSC growth to $M_{NSC} < 0.01 M_{BH}$.

The observed values of the NSC fraction are scattered over a large range. The median for the $M_* \lesssim 10^{11} M_{\odot}$

galaxies in Virgo and Fornax clusters is $M_{NSC}/M_* \approx 0.0036$ (Turner et al. 2012). The compilations of data for nearby galaxies by Seth et al. (2008) and Scott & Graham (2013) both have lower median values $M_{NSC}/M_* \approx 0.002$, and a scaling $M_{NSC} \propto \sigma_g^{2.1}$. On the other hand, Leigh et al. (2012) find a larger median fraction $M_{NSC}/M_* \approx 0.005$ and a steeper scaling $M_{NSC} \propto \sigma_g^{2.7}$, for 51 early-type galaxies in lower mass range $M_* < 2 \times 10^{10} M_{\odot}$. Given the large scatter for individual galaxies, on Figure 12 we plot only the median range $M_{NSC}/M_* = 0.002 - 0.005$.

While the NSC fraction decreases with galaxy mass, the fraction of mass remaining in bound globular clusters instead increases. M_{GC}/M_* ranges from about 0.001 at $M_* < 5 \times 10^{10} M_{\odot}$ to 0.005 at $M_* \sim 10^{12} M_{\odot}$, consistent with a compilation of many globular cluster systems by Harris et al. (2013), which has median $M_{GC}/M_* \sim 0.003$, again with large scatter for individual galaxies.

In addition to considering the mass enclosed within 10 pc, we also calculated the whole NSC density profile to the point where it drops below the density of field stars. Integrating to 40 pc from the center suffices for all of our models. We find that the half-mass radius of the whole NSC scales only weakly with mass, as $R_h \propto M_{NSC}^{0.23}$. The observed relation appears to be somewhat steeper, $R_h \propto M_{NSC}^{0.3-0.5}$ (Côté et al. 2006; Turner et al. 2012), which suggests that our calculations either overestimate the efficiency of dynamical friction, or underestimate the efficiency of direct cluster disruption.

6.4. Why is the Mass of Central Black Hole similar to the Mass of Globular Cluster System?

One of the initial motivations for this project was to investigate the puzzling similarity between the mass of the central black hole, M_{BH} , and the combined mass of the globular cluster system in a given galaxy, M_{GC} , discovered by Burkert & Tremaine (2010) in 16 early-type galaxies. Harris & Harris (2011) and Rhode (2012) doubled the sample size and confirmed this result. It is puzzling because globular clusters and central black holes currently occupy very different locations in their host galaxy.

What is the origin of the similarity of M_{BH} and M_{GC} ? We suggest that this correlation is not causal but secondary, resulting from both quantities being roughly proportional to the total galaxy mass including dark matter, M_h . For black holes it has been well established that $M_{BH} \propto M_*$ (see review by Kormendy & Ho 2013), and this relation could also be roughly expressed through total galaxy mass, as $M_{BH} \sim 10^{-4} M_h$. For globular clusters, Spitler & Forbes (2009) and Harris et al. (2013) showed that $M_{GC} \approx 6 \times 10^{-5} M_h$ across four orders of magnitude in galaxy mass (this scaling was first predicted in theoretical models using cosmological simulations by Kravtsov & Gnedin 2005). Thus the fractions of total galaxy mass contained in globular clusters and central black holes are indeed similar.

The processes of formation and evolution of black holes and globular clusters are undoubtedly complex. Is there any physical reason for the total galaxy mass being the primary, and only, predictor of their mass? One of the possible clues is suggested by the success of the abundance matching technique (Kravtsov & Klypin 1999; Colín et al. 1999; Neyrinck et al. 2004; Kravtsov et al. 2004; Vale & Ostriker 2004) in describing such varied properties of galaxy population as the redshift- and scale-dependent clustering strength,

average stellar density, and volume-averaged star formation rate (e.g., Behroozi et al. 2013b). In this technique, dark matter halos from cosmological simulations are matched to real galaxies in a rank-order relation, allowing for random scatter due to observational uncertainties in the derived luminosity functions at different redshifts. One of the main results of such modeling is the prediction that star formation in galaxies is very inefficient in general, allowing only a fraction of about 20% of the available baryons to be converted to stars in the most efficient galaxies (with $M_h \sim 10^{12} M_\odot$) and a much smaller fraction in the less-efficient galaxies. Such low fractions indicate that only central parts of halos are involved in building the observed stellar systems, including globular clusters and the material that eventually goes into the central black holes. The galactic environment (mergers, tidal interactions, etc.), although important in detail, appears to play a sub-dominant role to the halo mass. If this picture is correct, it explains why galaxy mass controls the properties of such distinct components as central black holes and extended globular cluster systems.

However, the growth of M_{BH} and M_{GC} with time may not be entirely unrelated to each other. Both could be growing most efficiently during the episodes of most active star formation, when the interstellar medium of the host galaxy is very gas-rich and pressurized. Such conditions could be realized, for example, during major mergers of gas-rich galaxies, as suggested for the formation of globular clusters by Muratov & Gnedin (2010).

7. SUMMARY

The observed profiles of globular cluster systems in normal galaxies are falling less rapidly with radius than the profiles of the spheroidal stellar component that has roughly the same age and metallicity distribution. This has been interpreted for some time as indicative of the depletion of GCs in the inner parts of galaxies due to dynamical processes – the principal one being dynamical friction, which drags massive GCs into the nuclear regions. We quantitatively estimate these processes, taking the initial GC distributions to be such that the clusters remaining at the present time fit current epoch observations. Thus, we find a good match to current GC properties for our galaxy and M87, which provides a consistency check for the model.

For the Milky Way the most probable value for the mass of the central cluster formed by this process is $(2-6)\times 10^7 M_{\odot}$ and size roughly $3-5\,\mathrm{pc}$. This is close to observational constraints for the mass and radius of the old stellar component at the Galactic center, making it probable that this feature of our galaxy was in fact formed from in-spiraling GCs. However, our model predicts a larger than observed density contrast of the NSC relative to the surrounding field stars, which may be a deficiency of the adopted field profile or the rate of dynamical friction.

Applying the same method to the giant elliptical galaxy M87, we obtain a NSC mass of $(3-10) \times 10^8 M_{\odot}$ and a radius of $5-8\,\mathrm{pc}$. In this calculation we allow for the late-time accretion of satellite systems, which would also contribute roughly $10^9 M_{\odot}$ in accreted black holes to M87, most of which would be expected to merge with the central BH, adding about 20% to its mass. We also construct evolutionary tracks for two smaller spheroidal stellar systems having masses of $M_* = 5 \times 10^{10} M_{\odot}$ and $2 \times 10^{11} M_{\odot}$, that produce NSCs of intermediate mass. Our results for NSC mass (Ta-

ble 1 and Figure 12) are consistent with the simple scaling $M_{NSC}/M_* \approx 0.0025 \, M_{*,11}^{-0.5}$. This result is plausible in that the globular cluster supply is roughly proportional to the spheroidal component, which would give a constant ratio, but the efficiency of dynamical friction decreases with the mass of the system, since the velocities go up and densities go down. Hence the NSC fraction is a declining function of spheroidal

Adopting a simple prescription that globular cluster formation was initiated at an epoch z = 6, we find that the time to assemble the nuclear clusters is relatively brief, ranging from 0.7 Gyr for the MW to 1.4 Gyr for M87. The stellar relaxation times in these systems are considerably shorter than the age, so that they would have sufficient time to reach the core-collapsed state where physical collisions among mainsequence stars or compact stellar objects are believed to lead to the formation of central BHs containing a non-negligible fraction of the cluster mass. This dynamical process may lead to the formation of seed BHs of mass $\sim 10^{-3}$ of the NSCs, which for our galaxy would be in the range $(2-5) \times 10^4 M_{\odot}$. For the much more massive systems such as M87, this process would give a seed mass of $(1-7) \times 10^5 M_{\odot}$. While only a tiny fraction of the final BH, it is amply large to allow episodic radiative accretion enough time to grow the central BH to its present mass. For example, a duty cycle of 4% (comparable to the fraction of high-redshift galaxies in AGN mode) with a Salpeter time of 5×10^7 yr allows a 10,000-fold increase in mass by z = 0. We find that the additional increase in mass due to accreted BHs (embedded in accreted satellite galaxies) is not dominant, but also not trivial (1/6 of the final BH mass), and the late-time mergers could give a possibly detectable gravitational wave signal (McWilliams et al. 2012).

It naturally follows from this scenario that essentially all galaxies with appreciable GC populations should host an old NSC, containing a fraction $\gtrsim 10^{-3}$ of the spheroidal stellar mass (as given by equation 13). The crossover galaxy mass, above which the central BH dominates over the NSC, appears to be at $M_* \sim 10^{11} M_{\odot}$. In addition to the clear prediction for the prevalence and properties of NSCs, this scenario also predicts the existence of a non-trivial number of satellite BHs orbiting massive galaxies, due to incomplete dynamical friction infall subsequent to minor mergers.

We would like to thank the referee for thoughtful comments that helped to clarify the description of nuclear core collapse, and Cole Miller for helpful discussions. We also thank Fabio Antonini, Roberto Capuzzo-Dolcetta, and Alister Graham for additional comments. O.Y.G. was supported in part by NASA through grant NNX12AG44G. S.T. was supported in part by NASA through grant NNX11AF29G. O.Y.G. thanks the Institute for Advanced Study in Princeton, Kavli Institute for Theoretical Physics in Santa Barbara, Kavli Institute for Cosmological Physics in Chicago, and Aspen Center for Physics for hospitality while this manuscript was being written.

REFERENCES

Agarwal, M. & Milosavljević, M. 2011, ApJ, 729, 35 Ambartsumian, V. A. 1938, Uch. Zap. Leningrad G. U., 22, 19 [English transl. in IAU Symp. 113, Dynamics of Star Clusters, ed. J. Goodman & P. Hut (Dordrecht: Reidel), 521] Antonini, F. 2013, ApJ, 763, 62

Antonini, F., Capuzzo-Dolcetta, R., Mastrobuono-Battisti, A., & Merritt, D. 2012, ApJ, 750, 111

Ascaso, B., Aguerri, J. A. L., Varela, J., Cava, A., Bettoni, D., Moles, M., & D'Onofrio, M. 2011, ApJ, 726, 69

Baumgardt, H. 2001, MNRAS, 325, 1323

Behroozi, P. S., Marchesini, D., Wechsler, R. H., Muzzin, A., Papovich, C., & Stefanon, M. 2013a, ApJ, 777, L10

Behroozi, P. S., Wechsler, R. H., & Conroy, C. 2013b, ApJ, 770, 57

Binney, J. & Tremaine, S. 2008, Galactic Dynamics (Princeton: Princeton University Press)

Bonatto, C. & Bica, E. 2012, MNRAS, 423, 1390

Boylan-Kolchin, M., Ma, C.-P., & Quataert, E. 2008, MNRAS, 383, 93 Breen, P. G. & Heggie, D. C. 2013a, MNRAS, 432, 2779

-. 2013b, MNRAS, 436, 584

Brodie, J. P., Romanowsky, A. J., Strader, J., & Forbes, D. A. 2011, AJ, 142,

Burkert, A. & Tremaine, S. 2010, ApJ, 720, 516

Capuzzo-Dolcetta, R. 1993, ApJ, 415, 616

Capuzzo-Dolcetta, R. & Mastrobuono-Battisti, A. 2009, A&A, 507, 183

Capuzzo-Dolcetta, R. & Miocchi, P. 2008, MNRAS, 388, L69

Chabrier, G. 2003, PASP, 115, 763

Chandar, R., Fall, S. M., & Whitmore, B. C. 2010a, ApJ, 711, 1263

Chandar, R., Whitmore, B. C., Calzetti, D., Di Nino, D., Kennicutt, R. C., Regan, M., & Schinnerer, E. 2011, ApJ, 727, 88

Chandar, R., Whitmore, B. C., Kim, H., Kaleida, C., Mutchler, M., Calzetti, D., Saha, A., O'Connell, R., Balick, B., Bond, H., Carollo, M., Disney, M., Dopita, M. A., Frogel, J. A., Hall, D., Holtzman, J. A., Kimble, R. A., McCarthy, P., Paresce, F., Silk, J., Trauger, J., Walker, A. R., Windhorst, R. A., & Young, E. 2010b, ApJ, 719, 966

Chernoff, D. F. & Weinberg, M. D. 1990, ApJ, 351, 121

Colín, P., Klypin, A. A., Kravtsov, A. V., & Khokhlov, A. M. 1999, ApJ, 523, 32,

Colpi, M., Mayer, L., & Governato, F. 1999, ApJ, 525, 720

Côté, P., Piatek, S., Ferrarese, L., Jordán, A., Merritt, D., Peng, E. W., Haşegan, M., Blakeslee, J. P., Mei, S., West, M. J., Milosavljević, M., & Tonry, J. L. 2006, ApJS, 165, 57

Fall, S. M. & Zhang, Q. 2001, ApJ, 561, 751

Gebhardt, K., Adams, J., Richstone, D., Lauer, T. R., Faber, S. M., Gültekin, K., Murphy, J., & Tremaine, S. 2011, ApJ, 729, 119

Gebhardt, K. & Thomas, J. 2009, ApJ, 700, 1690

Georgiev, I. Y., Puzia, T. H., Goudfrooij, P., & Hilker, M. 2010, MNRAS, 406, 1967

Gieles, M. 2009, MNRAS, 394, 2113

Gieles, M. & Baumgardt, H. 2008, MNRAS, 389, L28

Gieles, M., Heggie, D. C., & Zhao, H. 2011, MNRAS, 413, 2509

Glebbeek, E., Gaburov, E., de Mink, S. E., Pols, O. R., & Portegies Zwart, S. F. 2009, A&A, 497, 255

Gnedin, O. Y., Brown, W. R., Geller, M. J., & Kenyon, S. J. 2010, ApJ, 720, L108

Gnedin, O. Y., Lee, H. M., & Ostriker, J. P. 1999, ApJ, 522, 935

Graham, A. W. & Scott, N. 2013, ApJ, 764, 151

Gültekin, K., Richstone, D. O., Gebhardt, K., Lauer, T. R., Tremaine, S., Aller, M. C., Bender, R., Dressler, A., Faber, S. M., Filippenko, A. V., Green, R., Ho, L. C., Kormendy, J., Magorrian, J., Pinkney, J., & Siopis, C. 2009, ApJ, 698, 198

Guo, Y., McIntosh, D. H., Mo, H. J., Katz, N., van den Bosch, F. C., Weinberg, M., Weinmann, S. M., Pasquali, A., & Yang, X. 2009, MNRAS, 398, 1129

Gürkan, M. A., Freitag, M., & Rasio, F. A. 2004, ApJ, 604, 632

Harris, G. L. H. & Harris, W. E. 2011, MNRAS, 410, 2347

Harris, W. E. 1996, AJ, 112, 1487

Harris, W. E. 2001, in Star Clusters, Saas-Fee Advanced Course 28. Lecture Notes 1998, Swiss Society for Astrophysics and Astronomy. Edited by L. Labhardt and B. Binggeli (Springer-Verlag:Berlin), 223-408

Harris, W. E., Harris, G. L. H., & Alessi, M. 2013, ApJ, 772, 82

Hartmann, M., Debattista, V. P., Seth, A., Cappellari, M., & Quinn, T. R. 2011, MNRAS, 418, 2697

Hopkins, P. F., Bundy, K., Croton, D., Hernquist, L., Keres, D., Khochfar, S., Stewart, K., Wetzel, A., & Younger, J. D. 2010, ApJ, 715, 202

Hurley, J. R., Pols, O. R., & Tout, C. A. 2000, MNRAS, 315, 543 Jiang, C. Y., Jing, Y. P., Faltenbacher, A., Lin, W. P., & Li, C. 2008, ApJ,

675, 1095

Kormendy, J., Fisher, D. B., Cornell, M. E., & Bender, R. 2009, ApJS, 182,

Kormendy, J. & Ho, L. C. 2013, ARA&A, 51, 511

Kravtsov, A. V., Berlind, A. A., Wechsler, R. H., Klypin, A. A., Gottlöber, S., Allgood, B., & Primack, J. R. 2004, ApJ, 609, 35

Kravtsov, A. V. & Gnedin, O. Y. 2005, ApJ, 623, 650

Kravtsov, A. V. & Klypin, A. A. 1999, ApJ, 520, 437

Kruijssen, J. M. D. 2012, MNRAS, 426, 3008

Kruijssen, J. M. D. & Mieske, S. 2009, A&A, 500, 785

Kruijssen, J. M. D. & Portegies Zwart, S. F. 2009, ApJ, 698, L158

Kundu, A., Whitmore, B. C., Sparks, W. B., Macchetto, F. D., Zepf, S. E., & Ashman, K. M. 1999, ApJ, 513, 733

Lacey, C. & Cole, S. 1993, MNRAS, 262, 627

Larsen, S. S. 2009, A&A, 494, 539

Launhardt, R., Zylka, R., & Mezger, P. G. 2002, A&A, 384, 112

Leigh, N., Böker, T., & Knigge, C. 2012, MNRAS, 424, 2130

Leja, J., van Dokkum, P., & Franx, M. 2013, ApJ, 766, 33

Lotz, J. M., Telford, R., Ferguson, H. C., Miller, B. W., Stiavelli, M., & Mack, J. 2001, ApJ, 552, 572

Mandushev, G., Staneva, A., & Spasova, N. 1991, A&A, 252, 94 McLaughlin, D. E. 1999, AJ, 117, 2398

McLaughlin, D. E. & van der Marel, R. P. 2005, ApJS, 161, 304

McMillan, P. J. & Binney, J. J. 2010, MNRAS, 402, 934

McWilliams, S. T., Ostriker, J. P., & Pretorius, F. 2012, ApJ, submitted, arXiv:1211.5377

Merritt, D. 2009, ApJ, 694, 959

2010, ApJ, 718, 739

Miller, M. C. & Davies, M. B. 2012, ApJ, 755, 81

Misgeld, I. & Hilker, M. 2011, MNRAS, 414, 3699

Morscher, M., Umbreit, S., Farr, W. M., & Rasio, F. A. 2013, ApJ, 763, L15

Muratov, A. L. & Gnedin, O. Y. 2010, ApJ, 718, 1266

Naab, T., Johansson, P. H., & Ostriker, J. P. 2009, ApJ, 699, L178

Neumayer, N. & Walcher, C. J. 2012, Advances in Astronomy, 2012

Neyrinck, M. C., Hamilton, A. J. S., & Gnedin, N. Y. 2004, MNRAS, 348, 1 Nipoti, C., Treu, T., Leauthaud, A., Bundy, K., Newman, A. B., & Auger, M. W. 2012, MNRAS, 422, 1714

Noble, S. C., Krolik, J. H., & Hawley, J. F. 2009, ApJ, 692, 411

Oh, S., Kim, S. S., & Figer, D. F. 2009, Journal of Korean Astronomical Society, 42, 17

Oser, L., Naab, T., Ostriker, J. P., & Johansson, P. H. 2012, ApJ, 744, 63

Oser, L., Ostriker, J. P., Naab, T., Johansson, P. H., & Burkert, A. 2010, ApJ,

Paudel, S., Lisker, T., & Kuntschner, H. 2011, MNRAS, 413, 1764

Portegies Zwart, S. F. & McMillan, S. L. W. 2002, ApJ, 576, 899

Portegies Zwart, S. F., McMillan, S. L. W., & Gieles, M. 2010, ARA&A, 48,

Prieto, J. L. & Gnedin, O. Y. 2008, ApJ, 689, 919

Rhode, K. L. 2012, AJ, 144, 154

A&A, 469, 125

Rossa, J., van der Marel, R. P., Böker, T., Gerssen, J., Ho, L. C., Rix, H.-W., Shields, J. C., & Walcher, C.-J. 2006, AJ, 132, 1074

Sani, E., Marconi, A., Hunt, L. K., & Risaliti, G. 2011, MNRAS, 413, 1479 Schödel, R., Eckart, A., Alexander, T., Merritt, D., Genzel, R., Sternberg, A., Meyer, L., Kul, F., Moultaka, J., Ott, T., & Straubmeier, C. 2007,

Scott, N. & Graham, A. W. 2013, ApJ, 763, 76

Seth, A., Agüeros, M., Lee, D., & Basu-Zych, A. 2008, ApJ, 678, 116

Sippel, A. C. & Hurley, J. R. 2013, MNRAS, 430, L30

Spitler, L. R. & Forbes, D. A. 2009, MNRAS, 392, L1

Tamura, N., Sharples, R. M., Arimoto, N., Onodera, M., Ohta, K., & Yamada, Y. 2006, MNRAS, 373, 601

Thorne, K. S. 1974, ApJ, 191, 507

Tremaine, S. D., Ostriker, J. P., & Spitzer, Jr., L. 1975, ApJ, 196, 407 Turner, M. L., Côté, P., Ferrarese, L., Jordán, A., Blakeslee, J. P., Mei, S., Peng, E. W., & West, M. J. 2012, ApJS, 203, 5

Vale, A. & Ostriker, J. P. 2004, MNRAS, 353, 189

van den Bosch, F. C., Lewis, G. F., Lake, G., & Stadel, J. 1999, ApJ, 515, 50 van Dokkum, P. G., Whitaker, K. E., Brammer, G., Franx, M., Kriek, M.,

Labbé, I., Marchesini, D., Quadri, R., Bezanson, R., Illingworth, G. D., Muzzin, A., Rudnick, G., Tal, T., & Wake, D. 2010, ApJ, 709, 1018

Walsh, J. L., Barth, A. J., Ho, L. C., & Sarzi, M. 2013, ApJ, 770, 86

Waters, C. Z., Zepf, S. E., Lauer, T. R., Baltz, E. A., & Silk, J. 2006, ApJ, 650, 885

Yu. O. & Tremaine, S. 2002, MNRAS, 335, 965

Zhang, Q. & Fall, S. M. 1999, ApJ, 527, L81